DUSP1 promotes apoptosis and suppresses cell migration, while leaving the JIP1-protected cytokine production intact, during paramyxovirus infection.

Alexa C. Robitaille[1,2], Elise Caron[1], Nicolas Zucchini[1,3], Espérance Mukawera[1], Damien Adam[1,4], Mélissa K. Mariani[1], Anaïs Gélinas[1,3], Audray Fortin[1], Emmanuelle Brochiero[1,4] and Nathalie Grandvaux[1, 2 *]

[1] CRCHUM - Centre Hospitalier de l'Université de Montréal, 900 rue Saint Denis, Montréal, H2X 0A9, Qc, Canada

[2] Department of Biochemistry and Molecular Medicine, Faculty of Medicine, Université de Montréal, Québec, H3C 3J7, Canada

[3] Department of Microbiology, Infectiology and Immunology, Faculty of Medicine, Université de Montréal, Québec, H3C 3J7, Canada

[4] Department of Medicine, Faculty of Medicine, Université de Montréal, Québec, H3C 3J7, Canada

* Corresponding author: nathalie.grandvaux@umontreal.ca; Tel.: (+1) 514-890-8000 ext. 35292

Keywords: DUSP1, JIP1, JNK, p38, migration, apoptosis, Respiratory Syncytial Virus.

Running title: Antiviral defense against paramyxoviruses: role of DUSP1

Abstract

Paramyxoviruses include several pathogenic viruses, including respiratory syncytial virus (RSV). The cell autonomous antiviral response and proinflammatory cytokine secretion is key to limit viral spreading and orchestrate the subsequent immune response. This host defense must be strictly regulated to ensure a response of appropriate intensity and duration to eliminate the infection while limiting tissue damage that is associated with virus pathogenesis. Activation of the innate immune response is mainly dependent on signaling pathways leading to activation of the transcription factors NF-κB, IRF3 and AP-1. The activation and termination of the host antiviral defense is heavily regulated by post-translational modifications, most notably phosphorylation, implying that protein phosphatases are key negative regulators. Here, we investigated the role of the dual-specificity phosphatase 1 (DUSP1) in the regulation of the host defense against RSV and Sendai virus (SeV). We found that DUSP1 is upregulated during early SeV and RSV infections of A549 cells before being subjected to proteasomal degradation at later time points. We demonstrate that DUSP1 does not inhibit the cell autonomous antiviral response, but negatively regulates virus-induced JNK/p38 MAPK phosphorylation. Importantly, we found that interaction with the JNK-interacting protein (JIP) 1 scaffold protein protects a pool of JNK involved in AP-1 and cytokine production, from inhibition by DUSP1. Rather, DUSP1 promotes apoptosis, independently of JNK/p38 inhibition, and suppresses cell migration. Collectively, our data unveil a previously unrecognized selective role of DUSP1 in the regulation of functions associated with tissue damage and repair during paramyxovirus infections.

INTRODUCTION

The *Paramyxoviridae* family of ssRNA viruses includes several important human pathogens, amongst which respiratory syncytial virus (RSV) is a leading cause of acute lower respiratory tract infections (ARTIs) associated with morbidity and mortality in infants, children and elderly, but also adults of all-age with a compromised immune system, cardiopulmonary diseases or following transplantation [1, 2]. The capacity of infected cells to mount appropriate autonomous antiviral and proinflammatory responses against RNA viruses is critical to determine the outcome of the infection. As a consequence, the inability of the host to sustain an antiviral response leads to failure in eradicating the infection. Conversely, uncontrolled duration or intensity of the innate immune response is harmful to the host and is associated with the development of virus-associated pathogenesis, chronic inflammatory diseases and various autoimmune diseases [3, 4]. Therefore, these responses need to reach the ideal intensity and duration for efficient fighting of the infection while limiting tissue damage and promote tissue repair [5]. To this aim, the innate immune response is subjected to stringent regulation by both positive and negative regulatory mechanisms [6].

Upon virus entry and sensing by the cytosolic receptors retinoic acid-inducible gene I (RIG-I) and melanoma differentiation-associated protein 5 (MDA-5), the mitochondrial membrane-associated adaptor (MAVS) coordinates multiple signalling pathways ultimately leading to the activation of the transcription factors Interferon (IFN) regulatory factors (IRF) 3/7, Nuclear Factor κB (NF-κB) and Activator Protein 1 (AP-1) [7, 8, 9]. Activation of IRF3 relies on a complex set of phosphorylations mainly mediated by the TANK-binding kinase 1 (TBK1)/ IκB kinase epsilon (IKKε) kinases [10, 11, 12, 13, 14]. NF-κB, mainly p65/p50, activation during paramyxovirus infection occurs through IκB kinase (IKK)-dependent phosphorylation of the NF-

κB inhibitor protein IκBα and of the p65 subunit [15, 16]. The signaling cascade leading to AP-1 activation is more elusive, but ultimately results in the phosphorylation of the nuclear Activating Transcription Factor 2 (ATF-2) and c-Jun subunits by JNK and p38 Mitogen-Activated Protein Kinases (MAPK) [7, 17, 18]. The activation of these transcription factors promotes the transcription of early antiviral genes, type I/III Interferons (IFNs) and proinflammatory cytokines [9, 19, 20]. In response to IFNs, hundreds of interferon-stimulated genes (ISGs) are induced to limit virus replication through enhancement of virus detection and innate immune signaling, cytoskeleton remodeling, inhibition of protein translation, induction of apoptosis, amongst other antiviral functions [21, 22, 23].

Post-translational modifications (PTMs), including phosphorylation, ubiquitylation and acetylation, of signal transduction proteins involved in the pathways engaged downstream of virus sensing are crucial to reach a fine-tuned regulation of the innate immune response [24]. In light of the very well documented importance of phosphorylation PTMs in the regulation of this response, the identification of protein phosphatases negatively regulating these events has started to be unveiled. The exact role of the Ser/Thr protein phosphatase 1 (PP1) in the antiviral response remains elusive as PP1α and PP1γ were found to dephosphorylate MDA-5 and RIG-I leading to their activation [25], while they were also described to be responsible for the dephosphorylation of key C-terminal phosphoresidues of IRF3 leading to its inhibition [26]. Most likely reflecting the complexity of IRF3 regulation through phosphorylation at multiple C-terminal phosphoacceptor sites, two other phosphatases, the Ser/Thr protein phosphatase 2 (PP2A) and MAPK phosphatase (MKP) 5, dephosphorylate IRF3 to terminate its activation [27, 28, 29]. The Ser/Thr protein phosphatase, Mg^{2+}/Mn^{2+}-dependent (PPM) 1B acts as a TBK1 phosphatase to inhibit IRF3 activation, while PPM1A targets both TBK1/IKKε and MAVS for dephosphorylation to negatively regulate the antiviral response [30, 31].

In the present study, we sought to address the role of the MKP-1/DUSP1 dual phosphatase (referred to thereafter as DUSP1) in the regulation of the host-defense against the paramyxoviruses Sendai virus (SeV) and RSV. We demonstrate that DUSP1 is a negative regulator of virus-induced JNK/p38 MAPK phosphorylation. However, this function is neither linked to the inhibition of the cell autonomous antiviral response nor to the induction of a cytokine response elicited during virus infection. Interestingly, we found that sequestration of a pool of JNK by the JNK interacting protein 1 (JIP1) scaffold protein, previously shown to be critical for AP-1 and downstream cytokine production specifically, protects JNK from dephosphorylation by DUSP1. Although we confirmed that a JNK/p38 signalling module is involved in the induction of virus-induced apoptosis, DUSP1 appears to have a pro-apoptotic function independently of JNK and p38. Finally, we found that DUSP1 dampens cell migration. Altogether, these findings point to a previously unrecognized role of DUSP1 in functions that have an impact on virus-associated tissue damage and repair.

RESULTS

Induction of DUSP1 during SeV and RSV infection.

To first assess a potential function of DUSP1 during infection by paramyxoviruses, we analyzed DUSP1 expression during the course of SeV and RSV infection in A549 cells by immunoblot. DUSP1 was highly induced at 6 h of RSV infection, while induction during SeV infection was barely detectable (**Figure 1A**). In both infections, DUSP1 levels were significantly reduced at 24 h post-infection (**Figure 1A**). Because DUSP1 turnover was previously reported to be affected by the ubiquitin-proteasome pathway [32], we further analyzed DUSP1 levels during SeV and RSV infection in the presence of the 26S proteasome inhibitor MG132. In the presence of MG132, induction of DUSP1 is detectable in both infections and the overall DUSP1 levels were markedly

increased compared to control cells (**Figure 1B**). These results imply that DUSP1 protein levels are induced in response to paramyxovirus infection and that DUSP1 is subjected to proteasome-mediated degradation.

DUSP1 does not affect paramyxovirus replication

Next, we sought to determine whether DUSP1 belongs to the numerous negative regulators of the cell autonomous antiviral response induced in response to virus infections [6, 33]. First, because of their importance in the control of the antiviral defense, we evaluated whether DUSP1 has an impact on the signaling cascades leading to NF-κB and IRF3 activation. Considering previous characterization of NF-κB activation in the context of RSV infection [34], IκBα-S32 and p65-S536 phosphorylation were analyzed. Activation of IRF3 was monitored through detection of IRF3-S396 phosphorylation [35]. Ectopic expression of DUSP1 in A549 cells did not alter IκBα, p65 or IRF3 phosphorylation profiles observed during the course of SeV (**Figure 2A and B**) or RSV infection (**Figure 2C**), showing that DUSP1 does not play a role in the regulation of these defense pathways. Additionally, ectopic expression of DUSP1 in A549 cells neither significantly altered SeV N mRNA levels measured by qRT-PCR (**Figure 2D top panel**) nor the *de novo* production of RSV virions quantified by plaque assay (**Figure 2D bottom panel**). Consistently, RNAi-mediated silencing of DUSP1 did not alter the capacity of RSV to replicate in A549 cells (**Figure 2E**). Together these data indicate that DUSP1 does not negatively regulate the capacity of the cell to mount an autonomous antiviral response to restrict paramyxovirus replication.

DUSP1 inhibits paramyxovirus-induced JNK and p38 phosphorylation

Because DUSP1 preferentially dephosphorylates JNK and p38 in a variety of inflammatory contexts [36, 37], we next sought to evaluate the role of DUSP1 in the negative regulation of

paramyxovirus-induced JNK and p38 activation. First, we monitored the effect of ectopically expressed DUSP1 on the SeV- and RSV-induced JNK T183/Y185 and p38 T180/Y182 phosphorylation in A549 cells. As expected, immunoblot analysis revealed that SeV (**Figure 3A and B**), and to a lesser extent RSV (**Figure 3C**), induce JNK and p38 phosphorylation. Importantly, DUSP1 expression abrogates JNK and p38 phosphorylation (**Figure 3A-C**). Subsequently, we confirmed the role of DUSP1 through analysis of the impact of DUSP1 silencing on the profile of virus-induced JNK and p38 phosphorylation. Immunoblot analysis confirmed the efficiency of DUSP1 silencing in A549 cells throughout the course of SeV and RSV infection (**Figure 4**). Consistent with a role of DUSP1 in the dephosphorylation of JNK and p38, we observed a marked increase of JNK and p38 phosphorylation in the absence of DUSP1 during SeV (**Figure 4A**) and RSV infection (**Figure 4B**). Altogether, these observations reveal a critical role of DUSP1 in the negative regulation of JNK and p38 activation during paramyxovirus infection.

Interaction between JIP1 and JNK protects from DUSP1 dephosphorylation

Scaffolding proteins of the JNK-Interacting Proteins (JIP) family interact with distinct pools of JNK to specifically place them next to their upstream activators and downstream substrate mediating specific functional pathways [38, 39]. Therefore, we aimed to investigate the role of JIP proteins in paramyxovirus-induced JNK activation and regulation by DUSP1. The JIP family is composed of 4 members, JIP1-4, with distinct expression profiles. Here, we assessed the role of JIP1 and JIP3 in A549 cells based on previous reports indicative of their expression in lung cells [40, 41, 42, 43]. In contrary, JIP2 was shown to be restricted to human brain [44] and human JIP4 was found only in testis [45, 46]. First, we tested the interaction between JNK and JIP1 or JIP3 during SeV infection. Ectopically expressed JIP1 coimmunoprecipitated with endogenous JNK both in uninfected and SeV-infected cells (**Figure 5A**). By contrast, JIP3 did not interact with JNK

(**Figure 5A**). Since we demonstrated the existence of a JIP1/JNK complex, we examined the role of JIP1 in JNK phosphorylation and its capacity to be dephosphorylated by DUSP1 during SeV infection. A549 cells were cotransfected with JIP1 or JIP3 together with empty or DUSP1-expressing constructs before infection with SeV. Immunoblot analysis showed that ectopic expression of JIP1 led to increased JNK phosphorylation compared to control cells (**Figure 5B**). In contrary, reflecting the lack of interaction between JNK and JIP3, JNK phosphorylation remained unaffected by the ectopic expression of JIP3 (**Figure 5B**). Confirming our finding (**Figure 3**), ectopic expression of DUSP1 resulted in inhibition of JNK phosphorylation (**Figure 5B**). Interestingly, when JIP1 was coexpressed with DUSP1, the inhibition of JNK phosphorylation was only partial. Again, coexpression of JIP3 with DUSP1 did not alter the capacity of DUSP1 to dephosphorylate JNK. Collectively, these data demonstrate that JIP1 interacts with JNK and that recruitment of JNK by JIP1 ensures protection from dephosphorylation by DUSP1.

AP-1 and downstream cytokine production elicited during infection are protected from DUSP1-mediated inhibition of JNK and p38

JIP1 is essential for the activation of the JNK/c-Jun axis and downstream AP-1-dependent cytokine expression [47, 48, 49, 50]. A main function of JNK and p38 in the host defense against virus infection is to regulate the activation of AP-1 (ATF-2/c-Jun) that participates in the enhanceosome structure controlling IFNβ expression and contributes to the regulation of proinflammatory cytokine expression [7, 17, 18]. The observation that JIP1 is important to segregate JNK away from DUSP1 dephosphorylation suggests a model in which AP-1-dependent functions would be protected from the negative regulation of DUSP1 during the infection. To confirm that JNK/p38 were involved in paramyxovirus-induced AP-1 activation and downstream cytokine expression, A549 cells were infected with SeV in the absence or presence of JNK (SP600125)

and p38 (SB203580) inhibitors. Immunoblot analysis showed that inhibition of JNK and p38 significantly decreased the levels of phosphorylated c-Jun and ATF-2 (**Figure 6A**). Accordingly, inhibition of JNK and p38 significantly impaired the induction of IFNβ, CCL2, CXCL8 and IL-6 by SeV, quantified using Luminex-based assays (**Figure 6C and Supplemental Figure 1A**). These results confirmed the role of the JNK/p38-AP-1 signaling cascade in the regulation of SeV-mediated cytokine induction and therefore prompted us to evaluate the impact of ectopic expression of DUSP1 on this pathway. Although, ectopic expression of DUSP1 prevents JNK and p38 phosphorylation, SeV- and RSV-induced phosphorylation of c-Jun and ATF-2 remained similar to control cells (**Figure 6B and Supplemental Figure 2**). Analysis of the expression profile of a panel of 48 cytokines using Luminex-based multiplex assays during SeV infection revealed that none of them were significantly altered following DUSP1 ectopic expression (**Figure 6D and Supplemental Figure 1B**). Additionally, silencing of DUSP1 did not affect the levels of IFNβ, CCL2, CCL5, CXCL8 and IL-6 induced by SeV (**Figure 6E and Supplemental Figure 1C)**. Measurement of SeV-induced *IFNB, CXCL8* and *CCL2* mRNA levels revealed no impact of DUSP1 ectopic expression, excluding a role of DUSP1 in the transcriptional regulation of cytokines (**Supplemental Figure 3**). Altogether these observations point to a selective role of DUSP1 in the negative regulation of a specific pool of JNK and p38 during paramyxovirus infection, leaving the AP-1 pathway and downstream cytokine production intact.

DUSP1 promotes virus-induced apoptosis independently of JNK/p38 inhibition.

JNK/p38 MAPK pathways are also known to play a critical role in the regulation of apoptosis, being either pro- or anti-apoptotic depending on the context [51, 52, 53, 54, 55, 56]. A MAVS/JNK pathway has been shown to be indispensable for SeV to induce apoptosis [57, 58]. Therefore we sought to assess the impact of DUSP1 on the JNK/p38-dependent apoptosis triggered by SeV.

First, A549 cells were pretreated with DMSO (vehicle) or SP600125 and SB203580 to inhibit JNK and p38 before SeV infection and detection of apoptotic cells using Annexin V/PI staining. Flow cytometry-based quantification of Annexin V+ cells, corresponding to early and late apoptosis, revealed that inhibition of JNK/p38 significantly reduced SeV-induced apoptosis (**Figure 7A**). To investigate the relationship between the observed DUSP1-dependent inhibition of JNK/p38 phosphorylation and this pro-apoptotic function, apoptosis was next monitored during SeV infection following silencing of DUSP1. Unexpectedly, inhibition of DUSP1 expression significantly decreased apoptosis (**Figure 7B**). These findings confirmed that a JNK/p38 signaling module is involved in the induction of apoptosis during SeV infection, but they also argue against a negative regulation of this pathway by DUSP1. Rather, DUSP1 appears to have a pro-apoptotic function independently of JNK and p38.

DUSP1 negatively regulates cell migration during RSV infection.

Compelling evidence has implicated JNK/p38 in the positive regulation of cell migration in several cell types [59]. Phenotypic observation of A549 cells during RSV infection following DUSP1 silencing showed obvious formation of pseudopods that were not observed in control cells (**Supplementary Movie 1**). This pointed to a propensity of infected cells to stretch out and migrate in the absence of DUSP1. To investigate the role of DUSP1 in cell migration during virus infection, 2D cell migration dynamics was assessed by single-cell tracking using time-lapse video-microscopy in subconfluent A549 cell cultures infected with RSV following siCtrl or siDUSP1 transfection (**Supplementary Movie 1**). As hypothesized, cell trajectories and migration rates were altered following DUSP1 silencing. In the absence of DUSP1, cells were migrating further from their origin compared to control cells that rather adopted a trajectory in circles around their point of origin (**Figure 8**). These observations demonstrate a critical negative role of DUSP1 in the regulation of cell migration during paramyxovirus infection.

DISCUSSION

DUSP1 is expressed in various cell types and tissues and mainly acts as a critical negative regulator shaping the duration, magnitude and spatiotemporal profile of p38 and JNK MAPKs, and to a lesser extent ERK, activation following physiological and pathological stimuli [60]. As such, DUSP1 has been extensively shown to negatively regulate the innate immune anti-bacterial defense and the cellular response to allergens [61, 62]. In these contexts, DUSP1 mainly inhibits proinflammatory cytokine expression [37, 63, 64, 65, 66, 67, 68]. The role of DUSP1 in the innate response to virus infection is far less known and, to our knowledge, was not previously assessed in the context of infection by paramyxoviruses.

In the present study, we show that DUSP1 negatively regulates p38 and JNK phosphorylation induced by SeV and RSV (**Figure 3 and 4**). Analysis of virus replication as well as NF-κB and IRF3 signaling pathways excluded a role of DUSP1 in the negative regulation of the cell autonomous antiviral defense (**Figure 2**). The observation that pharmacological inhibition of JNK/p38 MAPKs during SeV infection significantly decreased downstream ATF-2/c-Jun activation and cytokine induction (**Figure 6A and C**) confirmed the previously documented existence of a JNK-p38/AP-1 signaling axis critical for virus-induced cytokine production [7, 17, 18]. Unexpectedly, DUSP1-mediated inhibition of JNK/p38 phosphorylation had no effect on downstream phosphorylation of ATF-2/c-Jun or on the levels of a wide panel of cytokines elicited during infection (**Figure 6**). We hypothesized that this observation might reflect the existence of different subsets of JNK segregated through the interaction with specific scaffold proteins. In the MAPK signaling modules involving JNK, members of the JIP family of scaffold proteins selectively enhance specific JNK-dependent functions by interacting with and linking the upstream kinases to JNK activation [38, 39]. In our experimental model, we showed that JNK

interacts with JIP1, but not with JIP3, at basal levels and during infection and that JIP1 enhances JNK phosphorylation (**Figure 5**). Importantly, we found that the JIP1/JNK interaction dampens the capacity of DUSP1 to dephosphorylate JNK (**Figure 5B**). Compelling evidence demonstrates that JIP1 is essential for the activation of the JNK/AP-1 axis that controls cytokine expression [47, 48, 49, 50]. Although we cannot exclude other mechanisms, it is reasonable to speculate that during paramyxovirus infection, the segregation of JNK through molecular interaction with JIP1 protects the subset of JNK involved in AP-1 and downstream cytokine induction from DUSP1 negative regulation (**Figure 6D**). Previous reports have shown that interaction with JIP1 leads to the retention of JNK in the cytoplasm [40, 69]. DUSP1 is a nuclear phosphatase [70, 71] and therefore predominantly dephosphorylates JNK and p38 in the nucleus [72]. It is thus very likely that retention of JNK in the cytoplasm by JIP1 contributes to protect JNK from DUSP1 dephosphorylation. Our results differ from previous reports showing DUSP1-dependent inhibition of IL-6 and CXCL8 expression following challenge with the viral dsRNA mimetic poly I:C or coronavirus infection [66, 73]. One might speculate that the JIP1/JNK interaction might be differently affected upon infection by distinct viruses. While we did not observe changes of the JIP1/JNK complex during SeV and RSV infection, other viruses may interfere with this interaction thereby making JNK available for dephosphorylation by DUSP1 to negatively regulate downstream cytokine release. Although to date no virus was reported to dissociate the JIP1/JNK complex, it is interesting to note that Vaccinia virus-encoded B1R kinase interacts with JIP1 leading to increased binding of JNK to JIP1 and downstream activation of c-Jun [74].

Amongst alternative functions driven by JNK and p38 MAPK pathways are the regulation of cell proliferation and apoptosis [75]. Cell cycle analysis during SeV and RSV infection following ectopic expression or silencing of DUSP1 failed to demonstrate a role of DUSP1 in cell

proliferation during paramyxovirus infection (data not shown). Instead, we found that DUSP1 is playing a pro-apoptotic function (**Figure 7B**). Confirming previous reports [57, 76, 77], we also found that inhibition of the JNK/p38 pathway impaired SeV-induced apoptosis (**Figure 7A**). Since both DUSP1 and JNK/p38 are part of pro-apoptotic pathways, it strongly hints at a model in which DUSP1 regulates virus-induced apoptosis in a JNK/p38-independent manner. Additionally, this also argues toward a model in which the JNK/p38 pro-apoptotic function is also protected from DUSP1 dephosphorylation, possibly through the observed JNK/JIP1 interaction. This model is consistent with the fact that MAVS-MKK7-JNK defines a pro-apoptotic pathway during SeV infection and that JIP1 specifically functions in the JNK pathway by tethering MLK3 (MAPKKK), MKK7 (MAPKK) and JNK [57, 69]. Moreover, the JIP1/JNK axis has also been shown to be pro-apoptotic in neurons exposed to stress [48, 78].

In the quest to characterize DUSP1-dependent JNK and p38 functions during paramyxovirus infection, we also assessed the impact of DUSP1 on cell migration. Indeed, accumulating evidence implicates JNK and p38 in pro-migratory functions in various contexts [59]. Here, we demonstrate that in the absence of DUSP1, cell migration of RSV infected cells was highly enhanced (**Figure 8**) pointing to a critical role of DUSP1 in the negative regulation of JNK and p38-mediated cell migration. Regulation of apoptosis and cell migration are part of the arsenal of the host response that have the potential to not only influence the outcome of virus spreading, but also the extent of virus-induced tissue damage and repair thereby contributing to pathogenesis [5, 79]. The implication of the observed DUSP1-mediated regulation of apoptosis and cell migration in paramyxovirus spreading can be excluded based on the lack of effect of DUSP1 ectopic expression or silencing on virus replication (**Figure 2**). Induction of apoptosis combined to inhibition of cell migration by DUSP1 rather suggests a role in the induction of cell damage and inhibition of tissue repair and thereby in virus-induced pathogenesis.

Altogether our results suggest a model in which DUSP1 is a negative regulator of important host mechanisms that limit tissue damage and promote tissue repair. An exaggerated cytokine response can also contribute to host self-inflicted damages and thereby contribute to virus-induced pathogenesis [80]. We found that the cytokine response remains intact upon manipulation of DUSP1 expression due to protection by the interaction of a subset of JNK with JIP1 (**Figure 5A**). The observation that JIP1/JNK interaction prevents a potential negative regulation of the cytokine response by DUSP1 opens avenues for specific therapeutic targeting. Indeed, one can hypothesize that inhibition of the JIP1/JNK interaction might restore DUSP1-dependent inhibition of the AP-1/cytokine axis during paramyxovirus infection, while leaving other JIP1-independent JNK functions unaffected. Further studies will be required to evaluate this possibility. The JIP1/JNK interaction has long been considered an interesting specific target and this led to the development of small molecules and peptides that inhibit the interaction between JNK and JIP1 and efficiently block JNK activity toward selective substrates, including ATF-2 and c-Jun [81, 82, 83, 84]. Alternatively, direct inhibition of DUSP1 [85, 86] might be a strategy to improve tissue homeostasis, by reducing virus-induced apoptosis and restoring cell migration, during virus infection.

MATERIALS AND METHODS

Cell culture

A549 cells (American Type Culture Collection, ATCC) were grown in Ham F12 medium (GIBCO) and Vero cells (ATCC) in Dulbecco's Modified Eagle Medium (DMEM, GIBCO). Both media were supplemented with 10 % heat-inactivated fetal bovine serum (HI-FBS, GIBCO) and 1 % L-Glutamine (GIBCO). Cultures were performed without antibiotics and were tested negative for

mycoplasma contamination (MycoAlert Mycoplasma Detection Kit, Lonza) every 2 months.

Infections

Subconfluent monolayers (90 % confluency) of A549 cells were infected with Sendai virus (SeV, Cantell strain, Charles River Laboratories) at 5-40 hemagglutinin units (HAU)/10^6 cells as indicated in serum free medium (SFM). At 2 h post-infection, the medium was supplemented with 10 % HI-FBS and the infection pursued for the indicated time. Infection with RSV A2 (Advanced Biotechnologies Inc), amplified and purified as described in [34], was performed at a MOI of 1-3 as indicated in medium containing 2 % HI-FBS. Where indicated, A549 were pretreated with 5 μM MG132 (Calbiochem) or DMSO (vehicle, Sigma-Aldrich) for 1 h before infection. Pretreatment with 10 μM SB203580 and 10 μM SP600125 (Invivogen) or the corresponding vehicle DMSO was performed for 30 min prior to infection.

SDS-PAGE and immunoblot

The procedures used for preparation of Whole Cell Extracts (WCE), resolution by SDS-PAGE electrophoresis and immunoblot was fully detailed in [87]. The following primary antibodies were used in this study: anti-MKP-1/DUSP1 (M18, #sc-1102), anti-α-tubulin (B-7, #sc-5286) and anti-NFκB p65 (C-20, #sc-372) were obtained from Santa Cruz Biotechnology. Anti-phosphoT183/Y185 SAPK/JNK (G9, #9255), anti-SAPK/JNK (#9252), anti-phosphoT180/Y182 p38 MAPK (D3F9, #4511), anti-p38 MAPK (D13E1, #8690), anti-phosphoS536 NF-kappaB p65 (93H1, #3033), anti-phosphoS32 IκBα (14D4, #2859), anti-IκBα (#9242), anti-phosphoT71 ATF-2 (11G2, #5112), anti-ATF-2 (20F1, #9226), anti-phosphoS73 c-Jun (D47G9, #3270) and anti-c-Jun (60A8, #9165) were from Cell Signaling. Anti-actin clone AC-15 (#A5441) and anti-Flag M2 (#F1804) were purchased from Sigma-Aldrich, anti-IRF3 (#39033) was from Active Motif and

anti-RSV (#AB1128) was from Chemicon International. Anti-phosphoS396 IRF3 was described in [35] and anti-SeV was obtained from Dr. J. Hiscott, McGill University, Montreal, Canada. HRP-conjugated goat anti-rabbit and rabbit anti-goat (Jackson Laboratories), and goat anti-mouse (Kirkegaard & Perry Laboratories) were used as secondary antibodies.

Plasmids

The human DUSP1-pCMV6XL5 plasmid was obtained from Origene. The pcdna3 Flag JIP1b (Addgene plasmid # 52123) and pcdna3 Flag JIP3b (Addgene plasmid # 53458) plasmids were a gift from Roger Davis [47, 88]. All constructs were verified using Sanger sequencing at the McGill University and Génome Québec Innovation Centre, Montréal, Canada.

Plasmid transfection

Plasmid transfection in A549 cells was achieved using the TransIT-LT1 transfection reagent (Mirus). Briefly, a total of 3 μg of DNA was transfected per 35 mm plates of A549 cells at 70 % confluency using a transfection reagent/DNA ratio of 1:2. Transfection was pursued for 24 h to 48 h before further treatment, as indicated.

qRT-PCR

Total RNA were extracted using the RNAqueous-96 Isolation Kit (Ambion) and quantified. Reverse transcription was performed using 1 μg total RNA using the Quantitect reverse Transcription kit (Qiagen). Specific mRNA levels were quantified by qPCR using Fast start SYBR Green Kit (Roche) for *SeV N* (S: agtatgggaggaccacagaatgg, AS: ccttcaccaacacaatccagacc). A reaction without RT and a reaction with H_2O were performed with each run to ensure absence of genomic DNA contamination. Fluorescence was collected using

the Rotor-Gene 3000 Real Time Thermal Cycler (Corbett Research). Results were analyzed by the ΔΔCT method after normalization to S9 mRNA levels (S: cgtctcgaccaagagctga, AS: ggtccttctcatcaagcgtc).

Virus titration by plaque forming unit (pfu) assay

RSV infectious virions were quantified by methylcellulose plaque forming units assay. Briefly, supernatant from infected plates was harvested and subjected to serial dilutions before being used to infect monolayers of Vero cells. After 2 h of infection, Vero cells were washed and covered with 1 % methylcellulose prepared in DMEM containing 2 % FBS. RSV plaques were immunodetected at 5 days post-infection. After removal of the methylcellulose, cells were fixed in 80 % methanol for 30 min and air-dried. Plates were incubated for 15 min at room temperature (RT) in PBS 0.1X pH 7.2 containing 2 % milk and 0.05 % tween before being incubated with anti-RSV antibodies (#AB1128, Chemicon International) for 3 h at RT, washed 3 times in PBS 0.1 X pH 7.2 containing 0.05 % tween and finally incubated with rabbit anti-goat antibodies (Jackson Laboratories) for 1 h at RT. After 3 more washes, plates were incubated with Enhanced Chemiluminescence substrate (ECL, Perkin Elmer Life Sciences) for 5 min at RT and chemiluminescence signal was detected using a CCD camera-based apparatus (LAS4000 mini, GE healthcare). Quantification of plaques was performed using the ImageQuantTL software (Molecular Dynamics) and expressed as pfu/ml.

RNAi transfection

RNAi oligonucleotide (ON-target siRNA, Dharmacon) transfection was performed using the Oligofectamine reagent (Invitrogen). A non-targeting sequence, described in [10], was used as control. For efficient DUSP1 expression silencing, a mix of two siRNA sequences, caguuauggugaugacuuauu and ccgacgacacauauacauauu, were used. Cells were plated at 30 %

confluency and transfected for 24-48 h before further treatment depending on specific experimental design.

Co-immunoprecipitation experiments

WCE were prepared as described in the immunoblot section. For co-immunoprecipitation studies, 1-1.5 mg of WCE were incubated with 2 μg anti-Flag M2 antibodies (#F1804, Sigma-Aldrich) linked to 30 μl protein G Sepharose beads (Sigma-Aldrich) for 3 h at 4 °C. Beads were washed 5 times with lysis buffer and the elution of immunocomplexes was performed by incubation with a solution of 100 μg/ml Flag peptide (#F3290, Sigma-Aldrich) prepared in lysis buffer for 2 h at 4 °C. Immunoprecipitates were then denatured with 1:4 (v/v) 5X loading buffer [87] and heated for 5 min at 100 °C. WCE and immunoprecipitates were resolved by SDS-PAGE as described in the immunoblot section.

Luminex-based quantification of cytokines

Supernatants from infected A549 cells were collected and centrifuged for 5 min at 1000 g followed by a 10 min centrifugation at 10 000 g to remove cell debris. Cytokines were quantified by Luminex xMAP Technology using the Bio-Plex Pro™ Human Cytokine Standard Plex Group I and Group II or custom assembled plex for IFNβ, IL-6, CXCL8, CCL2 or CCL5 from Bio-Rad on a Bio-Plex 200 System (Bio-Rad). Analyses were performed using the Bio-Plex Manager Software version 6.0.0.617. Heatmaps were produced from the raw expression analysis data using *R* [89] and the *gplots* package [90] on logarithmically transformed, centered and scaled data.

Detection of apoptosis by flow cytometry (Annexin V/PI staining)

For detection of apoptosis, the supernatant of cell culture was collected and cells were harvested using 0.05 % trypsin-EDTA. Supernatant and cells were pooled and centrifuged for 5 min at 250 g at 4 °C. The cell pellet was resuspended in Annexin V buffer (10 mM Hepes pH 7.4, 150 mM NaCl, 5 mM KCl, 1 mM $MgCl_2$ and 1.8 mM $CaCl_2$) and stained using 1 µl of FITC-Annexin V (#556419, BD Biosciences) and 1 µl of Propidium Iodide (PI, 1 mg/ml, #P-4170, Sigma-Aldrich) per 2-5 x 10^5 cells for 10 min at 4 °C. Immediately after staining, acquisition of fluorescence was performed on a BD LSR II flow cytometer (BD Biosciences) using the BD FACSDiva Software (BD Biosciences). A minimum of 10 000 cells was analyzed for each sample. Data were analyzed using the FlowJo software (FlowJo, LLC).

Analysis of cell migration

Two-dimensional cell migration of single cells (9 cells/picture and 4 pictures/condition) was evaluated by single-cell tracking using live-video microscopy. Images were captured at 5 min intervals over an 18 h period by digital camera connected to a Zeiss microscope (Axio Observer.Z1) as in [91]. The cell trajectories were analysed using the Image J software (National Institutes of Health, Bethesda, MD, USA).

Statistical analyses

Quantitative results are represented as mean +/- SEM. Statistical comparisons were performed with Prism 7 software (GraphPad) using the indicated tests. The following *P*-values were considered significant: P<0.05 (*), P<0.01 (**) or P<0.001 (***).

AUTHOR CONTRIBUTIONS

ACR, NZ, DA, EB and NG conceived and designed the experiments. ACR, EC, NZ, EM, DA, MM, AG and AF performed experiments. ACR, NZ, DA and NG analyzed the data. ACR and NG wrote the manuscript. All co-authors edited and approved the manuscript.

COMPETING FINANCIAL INTERESTS

The authors declare no competing financial interests.

Supplementary information is available at Cell Research's website.

REFERENCES

1. Russell, C.J. & Hurwitz, J.L. Sendai virus as a backbone for vaccines against RSV and other human paramyxoviruses. *Expert review of vaccines* **15**, 189-200 (2016).

2. Simoes, E.A. *et al.* Challenges and opportunities in developing respiratory syncytial virus therapeutics. *J Infect Dis* **211 Suppl 1**, S1-s20 (2015).

3. Baccala, R., Hoebe, K., Kono, D.H., Beutler, B. & Theofilopoulos, A.N. TLR-dependent and TLR-independent pathways of type I interferon induction in systemic autoimmunity. *Nat Med* **13**, 543-551 (2007).

4. Kato, H. & Fujita, T. RIG-I-like receptors and autoimmune diseases. *Curr Opin Immunol* **37**, 40-45 (2015).

5. Allie, S.R. & Randall, T.D. Pulmonary immunity to viruses. *Clinical science (London, England : 1979)* **131**, 1737-1762 (2017).

6. Quicke, K.M., Diamond, M.S. & Suthar, M.S. Negative regulators of the RIG-I-like receptor signaling pathway. *Eur J Immunol* **47**, 615-628 (2017).

7. Servant, M.J., Grandvaux, N. & Hiscott, J. Multiple signaling pathways leading to the activation of interferon regulatory factor 3. *Biochem Pharmacol* **64**, 985-992 (2002).

8. Taylor, K.E. & Mossman, K.L. Recent advances in understanding viral evasion of type I interferon. *Immunology* **138**, 190-197 (2013).

9. Yoneyama, M., Onomoto, K., Jogi, M., Akaboshi, T. & Fujita, T. Viral RNA detection by RIG-I-like receptors. *Curr Opin Immunol* **32**, 48-53 (2015).

10. Sharma, S. *et al.* Triggering the interferon antiviral response through an IKK-related pathway. *Science* **300**, 1148-1151. (2003).

11. Fitzgerald, K.A. *et al.* IKKepsilon and TBK1 are essential components of the IRF3 signaling pathway. *Nat Immunol* **4**, 491-496. (2003).

12. Clement, J.F. *et al.* Phosphorylation of IRF-3 on Ser 339 generates a hyperactive form of IRF-3 through regulation of dimerization and CBP association. *J Virol* **82**, 3984-3996 (2008).

13. Mori, M. *et al.* Identification of Ser-386 of interferon regulatory factor 3 as critical target for inducible phosphorylation that determines activation. *J Biol Chem* **279**, 9698-9702 (2004).

14. Fujii, K., Nakamura, S., Takahashi, K. & Inagaki, F. Systematic characterization by mass spectrometric analysis of phosphorylation sites in IRF-3 regulatory domain activated by IKK-i. *Journal of proteomics* **73**, 1196-1203 (2010).

15. Fink, K., Duval, A., Martel, A., Soucy-Faulkner, A. & Grandvaux, N. Dual role of NOX2 in respiratory syncytial virus- and sendai virus-induced activation of NF-kappaB in airway epithelial cells. *J Immunol* **180**, 6911-6922 (2008).

16. Liu, P. *et al.* Retinoic acid-inducible gene I mediates early antiviral response and Toll-like receptor 3 expression in respiratory syncytial virus-infected airway epithelial cells. *J Virol* **81**, 1401-1411 (2007).

17. Ford, E. & Thanos, D. The transcriptional code of human IFN-beta gene expression. *Biochim Biophys Acta* **1799**, 328-336 (2010).

18. Zhang, S. *et al.* The c-Jun N-terminal kinase (JNK) is involved in H5N1 influenza A virus RNA and protein synthesis. *Arch Virol* **161**, 345-351 (2016).

19. Gurtler, C. & Bowie, A.G. Innate immune detection of microbial nucleic acids. *Trends in microbiology* **21**, 413-420 (2013).

20. Dixit, E. & Kagan, J.C. Intracellular Pathogen Detection by RIG-I-Like Receptors. *Adv Immunol* **117**, 99-125 (2013).

21. Schneider, W.M., Chevillotte, M.D. & Rice, C.M. Interferon-stimulated genes: a complex web of host defenses. *Annual review of immunology* **32**, 513-545 (2014).

22. Li, M.M., MacDonald, M.R. & Rice, C.M. To translate, or not to translate: viral and host mRNA regulation by interferon-stimulated genes. *Trends in cell biology* **25**, 320-329 (2015).

23. Liu, S.Y., Sanchez, D.J. & Cheng, G. New developments in the induction and antiviral effectors of type I interferon. *Curr Opin Immunol* **23**, 57-64 (2011).

24. Chiang, C. & Gack, M.U. Post-translational Control of Intracellular Pathogen Sensing Pathways. *Trends in immunology* **38**, 39-52 (2017).

25. Wies, E. *et al.* Dephosphorylation of the RNA sensors RIG-I and MDA5 by the phosphatase PP1 is essential for innate immune signaling. *Immunity* **38**, 437-449 (2013).

26. Gu, M. *et al.* Protein phosphatase PP1 negatively regulates the Toll-like receptor- and RIG-I-like receptor-triggered production of type I interferon by inhibiting IRF3 phosphorylation at serines 396 and 385 in macrophage. *Cell Signal* **26**, 2930-2939 (2014).

27. Long, L. *et al.* Recruitment of phosphatase PP2A by RACK1 adaptor protein deactivates transcription factor IRF3 and limits type I interferon signaling. *Immunity* **40**, 515-529 (2014).

28. James, Sharmy J. *et al.* MAPK Phosphatase 5 Expression Induced by Influenza and Other RNA Virus Infection Negatively Regulates IRF3 Activation and Type I Interferon Response. *Cell Reports* **10**, 1722-1734 (2015).

29. Peng, D., Wang, Z., Huang, A., Zhao, Y. & Qin, F.X. A Novel Function of F-Box Protein FBXO17 in Negative Regulation of Type I IFN Signaling by Recruiting PP2A for IFN Regulatory Factor 3 Deactivation. *J Immunol* **198**, 808-819 (2017).

30. Zhao, Y. *et al.* PPM1B negatively regulates antiviral response via dephosphorylating TBK1. *Cell Signal* **24**, 2197-2204 (2012).

31. Xiang, W., Zhang, Q. & Lin, X. PPM1A silences cytosolic RNA sensing and antiviral defense through direct dephosphorylation of MAVS and TBK1. **2**, e1501889 (2016).

32. Lin, Y.W., Chuang, S.M. & Yang, J.L. ERK1/2 achieves sustained activation by stimulating MAPK phosphatase-1 degradation via the ubiquitin-proteasome pathway. *J Biol Chem* **278**, 21534-21541 (2003).

33. Eisenacher, K. & Krug, A. Regulation of RLR-mediated innate immune signaling--it is all about keeping the balance. *Eur J Cell Biol* **91**, 36-47 (2012).

34. Yoboua, F., Martel, A., Duval, A., Mukawera, E. & Grandvaux, N. Respiratory syncytial virus-mediated NF-kappa B p65 phosphorylation at serine 536 is dependent on RIG-I, TRAF6, and IKK beta. *J Virol* **84**, 7267-7277 (2010).

35. Servant, M.J. *et al.* Identification of the minimal phosphoacceptor site required for in vivo activation of interferon regulatory factor 3 in response to virus and double-stranded RNA. *J Biol Chem* **278**, 9441-9447 (2003).

36. Franklin, C.C. & Kraft, A.S. Conditional expression of the mitogen-activated protein kinase (MAPK) phosphatase MKP-1 preferentially inhibits p38 MAPK and stress-activated protein kinase in U937 cells. *J Biol Chem* **272**, 16917-16923 (1997).

37. Zhao, Q. *et al.* The role of mitogen-activated protein kinase phosphatase-1 in the response of alveolar macrophages to lipopolysaccharide: attenuation of proinflammatory cytokine biosynthesis via feedback control of p38. *J Biol Chem* **280**, 8101-8108 (2005).

38. Dhanasekaran, D.N., Kashef, K., Lee, C.M., Xu, H. & Reddy, E.P. Scaffold proteins of MAP-kinase modules. *Oncogene* **26**, 3185-3202 (2007).

39. Zeke, A., Misheva, M., Remenyi, A. & Bogoyevitch, M.A. JNK Signaling: Regulation and Functions Based on Complex Protein-Protein Partnerships. *Microbiol Mol Biol Rev* **80**, 793-835 (2016).

40. Dickens, M. *et al.* A cytoplasmic inhibitor of the JNK signal transduction pathway. *Science* **277**, 693-696 (1997).

41. Di, A. *et al.* A novel function of sphingosine kinase 1 suppression of JNK activity in preventing inflammation and injury. *J Biol Chem* **285**, 15848-15857 (2010).

42. Kelkar, N. *et al.* Morphogenesis of the telencephalic commissure requires scaffold protein JNK-interacting protein 3 (JIP3). *Proc Natl Acad Sci U S A* **100**, 9843-9848 (2003).

43. Desai, L.P., White, S.R. & Waters, C.M. Mechanical stretch decreases FAK phosphorylation and reduces cell migration through loss of JIP3-induced JNK phosphorylation in airway epithelial cells. *Am J Physiol Lung Cell Mol Physiol* **297**, L520-529 (2009).

44. Yasuda, J., Whitmarsh, A.J., Cavanagh, J., Sharma, M. & Davis, R.J. The JIP group of mitogen-activated protein kinase scaffold proteins. *Mol Cell Biol* **19**, 7245-7254 (1999).

45. Shankar, S., Mohapatra, B. & Suri, A. Cloning of a novel human testis mRNA specifically expressed in testicular haploid germ cells, having unique palindromic sequences and encoding a leucine zipper dimerization motif. *Biochem Biophys Res Commun* **243**, 561-565 (1998).

46. Yasuoka, H. *et al.* A Novel Protein Highly Expressed in Testis Is Overexpressed in Systemic Sclerosis Fibroblasts and Targeted by Autoantibodies. *The Journal of Immunology* **171**, 6883-6890 (2003).

47. Whitmarsh, A.J., Cavanagh, J., Tournier, C., Yasuda, J. & Davis, R.J. A Mammalian Scaffold Complex That Selectively Mediates MAP Kinase Activation. *Science* **281**, 1671-1674 (1998).

48. Whitmarsh, A.J. *et al.* Requirement of the JIP1 scaffold protein for stress-induced JNK activation. *Genes Dev* **15**, 2421-2432 (2001).

49. Melino, M., Hii, C.S., McColl, S.R. & Ferrante, A. The effect of the JNK inhibitor, JIP peptide, on human T lymphocyte proliferation and cytokine production. *J Immunol* **181**, 7300-7306 (2008).

50. Blanco, S., Sanz-Garcia, M., Santos, C.R. & Lazo, P.A. Modulation of interleukin-1 transcriptional response by the interaction between VRK2 and the JIP1 scaffold protein. *PLoS One* **3**, e1660 (2008).

51. Ventura, J.J. *et al.* Chemical genetic analysis of the time course of signal transduction by JNK. *Mol Cell* **21**, 701-710 (2006).

52. Arbour, N. *et al.* c-Jun NH(2)-Terminal Kinase (JNK)1 and JNK2 Signaling Pathways Have Divergent Roles in CD8(+) T Cell–mediated Antiviral Immunity. *The Journal of Experimental Medicine* **195**, 801-810 (2002).

53. Zhang, H. *et al.* Activation of PI3K/Akt pathway limits JNK-mediated apoptosis during EV71 infection. *Virus Research* **192**, 74-84 (2014).

54. Gillis, P.A., Okagaki, L.H. & Rice, S.A. Herpes Simplex Virus Type 1 ICP27 Induces p38 Mitogen-Activated Protein Kinase Signaling and Apoptosis in HeLa Cells. *Journal of Virology* **83**, 1767-1777 (2009).

55. Liu, J. & Lin, A. Role of JNK activation in apoptosis: A double-edged sword. *Cell Res* **15**, 36-42 (2005).

56. Shiizaki, S., Naguro, I. & Ichijo, H. Activation mechanisms of ASK1 in response to various stresses and its significance in intracellular signaling. *Advances in Biological Regulation* **53**, 135-144 (2013).

57. Huang, Y. *et al.* MAVS-MKK7-JNK2 Defines a Novel Apoptotic Signaling Pathway during Viral Infection. *PLoS Pathog* **10**, e1004020 (2014).

58. Mosallanejad, K. *et al.* The DEAH-box RNA helicase DHX15 activates NF-kappaB and MAPK signaling downstream of MAVS during antiviral responses. *Sci Signal* **7**, ra40 (2014).

59. Huang, C., Jacobson, K. & Schaller, M.D. MAP kinases and cell migration. *J Cell Sci* **117**, 4619-4628 (2004).

60. Korhonen, R. & Moilanen, E. Mitogen-activated protein kinase phosphatase 1 as an inflammatory factor and drug target. *Basic & clinical pharmacology & toxicology* **114**, 24-36 (2014).

61. Wang, X. & Liu, Y. Regulation of innate immune response by MAP kinase phosphatase-1. *Cellular Signalling* **19**, 1372-1382 (2007).

62. Clark, A.R. MAP kinase phosphatase 1: a novel mediator of biological effects of glucocorticoids? *The Journal of endocrinology* **178**, 5-12 (2003).

63. Smallie, T. *et al.* Dual-Specificity Phosphatase 1 and Tristetraprolin Cooperate To Regulate Macrophage Responses to Lipopolysaccharide. *J Immunol* **195**, 277-288 (2015).

64. Chi, H. *et al.* Dynamic regulation of pro- and anti-inflammatory cytokines by MAPK phosphatase 1 (MKP-1) in innate immune responses. *Proc Natl Acad Sci U S A* **103**, 2274-2279 (2006).

65. Xiao, j. *et al.* MiR-429 Regulates Alveolar Macrophage Inflammatory Cytokine Production and is Involved in LPS-induced Acute Lung Injury. *Biochemical Journal* (2015).

66. Golebski, K. *et al.* EGR-1 and DUSP-1 are important negative regulators of pro-allergic responses in airway epithelium. *Mol Immunol* **65**, 43-50 (2015).

67. Salojin, K.V. *et al.* Essential Role of MAPK Phosphatase-1 in the Negative Control of Innate Immune Responses. *The Journal of Immunology* **176**, 1899-1907 (2006).

68. Abraham, S.M. *et al.* Antiinflammatory effects of dexamethasone are partly dependent on induction of dual specificity phosphatase 1. *J Exp Med* **203**, 1883-1889 (2006).

69. Moon, J. & Park, S.H. Reassembly of JIP1 scaffold complex in JNK MAP kinase pathway using heterologous protein interactions. *PLoS One* **9**, e96797 (2014).

70. Caunt, C.J. & Keyse, S.M. Dual-specificity MAP kinase phosphatases (MKPs): shaping the outcome of MAP kinase signalling. *Febs j* **280**, 489-504 (2013).

71. Kondoh, K. & Nishida, E. Regulation of MAP kinases by MAP kinase phosphatases. *Biochimica et Biophysica Acta (BBA) - Molecular Cell Research* **1773**, 1227-1237 (2007).

72. Zehorai, E. & Seger, R. Beta-like importins mediate the nuclear translocation of mitogen-activated protein kinases. *Mol Cell Biol* **34**, 259-270 (2014).

73. Liao, Y., Wang, X., Huang, M., Tam, J.P. & Liu, D.X. Regulation of the p38 mitogen-activated protein kinase and dual-specificity phosphatase 1 feedback loop modulates the induction of interleukin 6 and 8 in cells infected with coronavirus infectious bronchitis virus. *Virology* **420**, 106-116 (2011).

74. Santos, C.R., Blanco, S., Sevilla, A. & Lazo, P.A. Vaccinia virus B1R kinase interacts with JIP1 and modulates c-Jun-dependent signaling. *J Virol* **80**, 7667-7675 (2006).

75. Sun, Y. *et al.* Signaling pathway of MAPK/ERK in cell proliferation, differentiation, migration, senescence and apoptosis. *Journal of receptor and signal transduction research* **35**, 600-604 (2015).

76. Zhang, Q. *et al.* IPS-1 plays a dual function to directly induce apoptosis in murine melanoma cells by inactivated Sendai virus. *Int J Cancer* **134**, 224-234 (2014).

77. Gao, H. *et al.* Induction of apoptosis in hormone-resistant human prostate cancer PC3 cells by inactivated Sendai virus. *Biomedical and environmental sciences : BES* **27**, 506-514 (2014).

78. Kim, A.H. *et al.* Akt1 regulates a JNK scaffold during excitotoxic apoptosis. *Neuron* **35**, 697-709 (2002).

79. Barber, G.N. Host defense, viruses and apoptosis. *Cell death and differentiation* **8**, 113-126. (2001).

80. Tisoncik, J.R. *et al.* Into the eye of the cytokine storm. *Microbiol Mol Biol Rev* **76**, 16-32 (2012).

81. Stebbins, J.L. *et al.* Identification of a new JNK inhibitor targeting the JNK-JIP interaction site. *Proc Natl Acad Sci U S A* **105**, 16809-16813 (2008).

82. Bonny, C., Oberson, A., Negri, S., Sauser, C. & Schorderet, D.F. Cell-Permeable Peptide Inhibitors of JNK. *Novel Blockers of β-Cell Death* **50**, 77-82 (2001).

83. Barr, R.K., Kendrick, T.S. & Bogoyevitch, M.A. Identification of the critical features of a small peptide inhibitor of JNK activity. *J Biol Chem* **277**, 10987-10997 (2002).

84. Borsello, T. *et al.* A peptide inhibitor of c-Jun N-terminal kinase protects against excitotoxicity and cerebral ischemia. *Nat Med* **9**, 1180-1186 (2003).

85. Vogt, A. *et al.* The benzo[c]phenanthridine alkaloid, sanguinarine, is a selective, cell-active inhibitor of mitogen-activated protein kinase phosphatase-1. *J Biol Chem* **280**,

19078-19086 (2005).

86. Chen, P. *et al.* Restraint of proinflammatory cytokine biosynthesis by mitogen-activated protein kinase phosphatase-1 in lipopolysaccharide-stimulated macrophages. *J Immunol* **169**, 6408-6416 (2002).

87. Robitaille, A.C., Mariani, M.K., Fortin, A. & Grandvaux, N. A High Resolution Method to Monitor Phosphorylation-dependent Activation of IRF3. *J Vis Exp*, e53723 (2016).

88. Kelkar, N., Gupta, S., Dickens, M. & Davis, R.J. Interaction of a mitogen-activated protein kinase signaling module with the neuronal protein JIP3. *Mol Cell Biol* **20**, 1030-1043 (2000).

89. Team, R.C. R: A language and environment for statistical computing. Vienna, Austria: R Foundation for Statistical Computing; 2016.

90. Warnes, G.R. *et al.* gplots: Various R Programming Tools for Plotting Data. R package version 3.0.1. (2016).

91. Girault, A. *et al.* Complementary roles of KCa3.1 channels and beta1-integrin during alveolar epithelial repair. *Respiratory research* **16**, 100 (2015).

ACKNOWLEDGEMENTS

We thank members of the laboratory and of the immunovirology group at CRCHUM for fruitful discussions. We also thank François-Christophe Marois-Blanchet and François Harvey at the CRCHUM bioinformatics facility and Dr. Dominique Gauchat and Annie Gosselin at the CRCHUM flow cytometry platform.

The present work was funded by grants from the Canadian Institutes of Health Research (CIHR) [MOP-130527] and by the Research Chair in signaling in virus infection and oncogenesis from the Université de Montréal to NG. ACR was supported by graduate studentships from CIHR and the Fonds de la Recherche du Québec en Santé (FRQS) and AG by a studentship from Natural Sciences and Engineering Research Council of Canada (NSERC). NZ was recipient of a post-doctoral fellowship from FRQS/INSERM (Québec/France) and DA by a post-doctoral fellowship from FRQS. NG was recipient of a Tier II Canada Research Chair.

TITLES AND LEGENDS TO FIGURES

Figure 1: DUSP1 is induced during SeV and RSV infections and subjected to proteasomal degradation.

In **A and B,** A549 cells were infected with SeV at 40 HAU/10^6 cells or RSV at a MOI of 3 for the indicated times. **In B,** cells were pre-treated with MG132 (5 μM) or DMSO (vehicle) before infection for 6 h. WCE were analyzed by immunoblot using anti-DUSP1 specific antibodies. Detection of tubulin was used to control for equal loading. The data are representative of at least three independent experiments. NS: non-specific.

Figure 2: DUSP1 expression does not alter the antiviral pathways triggered by paramyxovirus infections.

A549 cells were transfected with an empty- or DUSP1-expressing plasmid **(A-D)** or with Ctrl or DUSP1 specific siRNA **(E)** before infection with SeV at 40 **(A and B)** or 5 HAU/10^6 cells (**D, top panel**) or with RSV at MOI of 3 **(C)** or 1 **(D, bottom panel and E)** for the indicated times. In **A-C,** immunoblot analyses were performed to detect DUSP1, phosphorylated p65 (p65-P), total p65, phosphorylated IκBα (IκBα-P), total IκBα, phosphorylated IRF3 (IRF3-P) and total IRF3. Infection was monitored using anti-SeV or anti-RSV antibodies (N proteins are shown). Detection of actin was used as a loading control. The data are representative of three different experiments. **In D,** SeV N mRNA was quantified by qRT-PCR. In **D and E,** the release of infectious RSV virions was quantified by plaque forming unit (pfu) assay. Data are represented as mean +/- SEM of n=6 **(D, top panel)** or n=8 **(D, bottom panel and E)** and analyzed using two-way ANOVA.

Figure 3: Ectopic expression of DUSP1 inhibits JNK and p38 phosphorylation elicited by SeV and RSV infections.

A549 cells were transfected with an empty- or DUSP1-encoding plasmid before infection with SeV at 40 HAU/10^6 cells **(A and B)** or RSV at a MOI of 3 **(C)** for the indicated times. Levels of DUSP1, phosphorylated JNK (JNK-P), total JNK, phosphorylated p38 (p38-P), total p38, SeV N and RSV N protein levels were monitored by immunoblot. Equal loading was verified using anti-tubulin antibodies. The data are representative of at least three independent experiments. NS: non-specific.

Figure 4: DUSP1 silencing increases paramyxovirus-induced JNK and p38 phosphorylation.

A549 cells were transfected with Ctrl or DUSP1-specific siRNA before being left uninfected or infected with SeV at 40 HAU/10^6 cells **(A)** or RSV at MOI of 3 **(B)** for various times. Immunoblot analyses were performed to verify the efficiency of DUSP1 silencing and expression levels of phosphorylated JNK (JNK-P), total JNK, phosphorylated p38 (p38-P) and total p38. Infection was monitored using anti-SeV and anti-RSV antibodies (N proteins are shown). Detection of actin was used as a loading control. The data are representative of at least three independent experiments. NS: non-specific.

Figure 5: JIP1 scaffold interacts with JNK and protects from dephosphorylation by DUSP1.

A549 cells were transfected with the indicated combination of Flag-JIP1-, Flag-JIP3- and DUSP1-expressing plasmids or the corresponding empty plasmids, and left uninfected or infected with SeV at 40 HAU/10^6 cells for 6 h. In **A,** WCE were subjected to immunoprecipitation (IP) using anti-Flag antibodies followed by Immunoblot. In **B,** WCE were resolved by SDS-PAGE

before immunoblot. In **A and B,** levels of protein expression were assessed using anti-Flag, anti-phosphorylated JNK (JNK-P), anti-JNK and anti-DUSP1 antibodies. Tubulin was used as a loading control. Data are representative of three different experiments. NS: non-specific.

Figure 6: DUSP1-mediated inhibition of JNK and p38 leaves virus-mediated activation of AP-1 and cytokine production intact.

A549 cells were either pretreated with DMSO (vehicle) or SB203580 (10 μM) + SP600125 (10 μM) for 30 min prior to infection **(A and C)**, transfected with empty or DUSP1-expressing plasmids **(B and D)** or transfected with Control (siCtrl) or DUSP1-specific siRNA **(E)** before infection with SeV at 40 HAU/10^6 cells for the indicated times or for 6 h **(A and C)**, 16 h **(D)** or 12 h **(E)**. In **A and B,** levels of phosphorylated ATF-2 (ATF-2-P), total ATF-2, phosphorylated c-Jun (c-Jun-P), total c-Jun and DUSP1 were analyzed by immunoblot. Actin was used to verify equal loading. The data are representative of three independent experiments. In **C-E,** release of cytokines was quantified using Luminex-based multiplex assays. Heatmap represents cytokine levels (pg/ml) logarithmically transformed, centered and scaled, measured in each biological replicates (n=3 in **C** and **E**, n=6 in **D**). Scatter plots of cytokines levels are shown in **Supplemental Figure 1**.

Figure 7: DUSP1 and JNK/p38 act on independent SeV-induced proapoptotic pathways.

A549 cells were pretreated with DMSO (vehicle) or SB203580 + SP600125 (10 μM each) for 30 min before infection **(A)** or transfected with control (siCtrl) or DUSP1-specific siRNA prior to infection **(B)**. SeV infection was performed at 40 HAU/10^6 cells for 8 h. Cells were harvested and double-stained with Annexin V-FITC and PI and analyzed by flow cytometry. The left bar graphs represent the percentage of Annexin V positive (Annexin V^+ / PI^- and Annexin V^+ / PI^+; Q2 and

Q3) apoptotic cells. Data are represented as mean +/- SEM of n≥3 independent replicates and analyzed by unpaired t-test. Representative FACS plots are shown.

Figure 8: DUSP1 blocks cell migration during RSV infection.

A549 cells were transfected with control (siCtrl) or DUSP1-specific siRNA before RSV infection at a MOI of 3 for 8 h. Single-cell tracking was performed using live-video microscopy to monitor two-dimensional cell migration. Trajectories of 9 cells per conditions are presented. The origins of cell trajectories have been aligned to start to the origin (x = 0; y = 0). The data are representative of two independent experiments. Original live video imaging of cell tracking are available in **Supplementary Movie 1**.

Figure 1

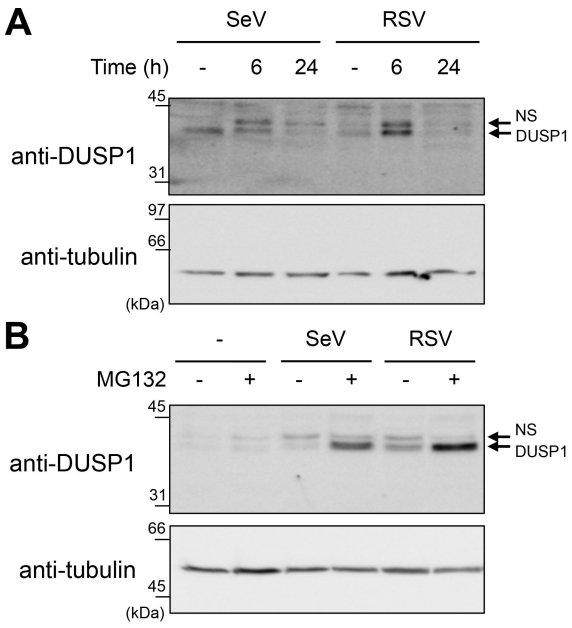
A
SeV
RSV
Time (h)
-
6
24
-
6
24
45
31
anti-DUSP1
NS
DUSP1
97
66
anti-tubulin
(kDa)
B
-
SeV
RSV
MG132
-
+
-
+
-
+
45
31
anti-DUSP1
NS
DUSP1
66
45
anti-tubulin
(kDa)

Figure 2

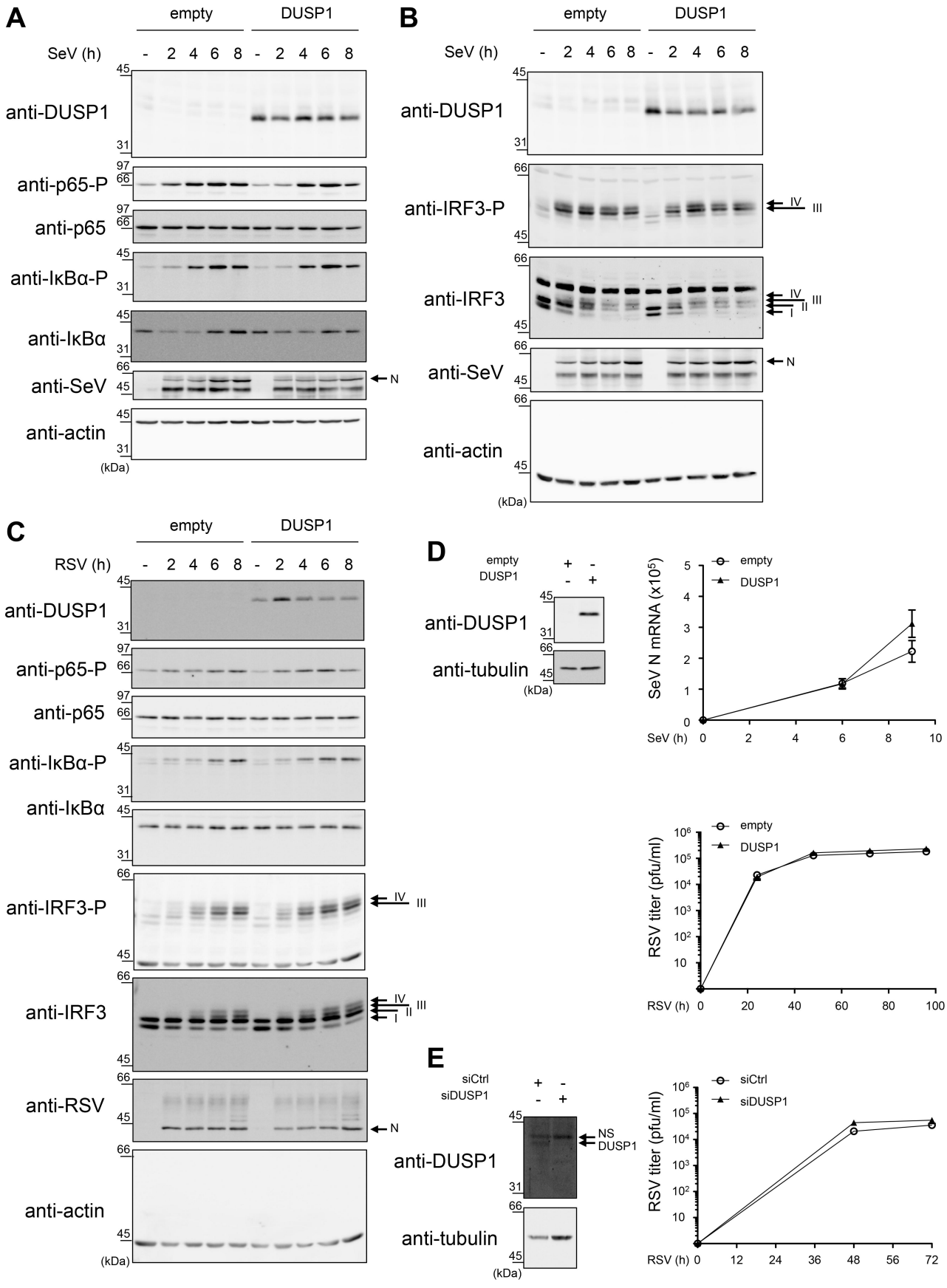
A
empty
DUSP1
SeV (h)
- 2 4 6 8 - 2 4 6 8
anti-DUSP1
anti-p65-P
anti-p65
anti-IκBα-P
anti-IκBα
anti-SeV
anti-actin
N
(kDa)
B
empty
DUSP1
SeV (h)
- 2 4 6 8 - 2 4 6 8
anti-DUSP1
anti-IRF3-P
anti-IRF3
anti-SeV
anti-actin
IV
III
II
I
N
(kDa)
C
empty
DUSP1
RSV (h)
- 2 4 6 8 - 2 4 6 8
anti-DUSP1
anti-p65-P
anti-p65
anti-IκBα-P
anti-IκBα
anti-IRF3-P
anti-IRF3
anti-RSV
anti-actin
IV
III
II
I
N
(kDa)
D
empty
DUSP1
anti-DUSP1
anti-tubulin
(kDa)
SeV N mRNA (x10^5)
SeV (h)
empty
DUSP1
RSV titer (pfu/ml)
RSV (h)
empty
DUSP1
E
siCtrl
siDUSP1
anti-DUSP1
anti-tubulin
NS
DUSP1
(kDa)
RSV titer (pfu/ml)
RSV (h)
siCtrl
siDUSP1

Figure 3

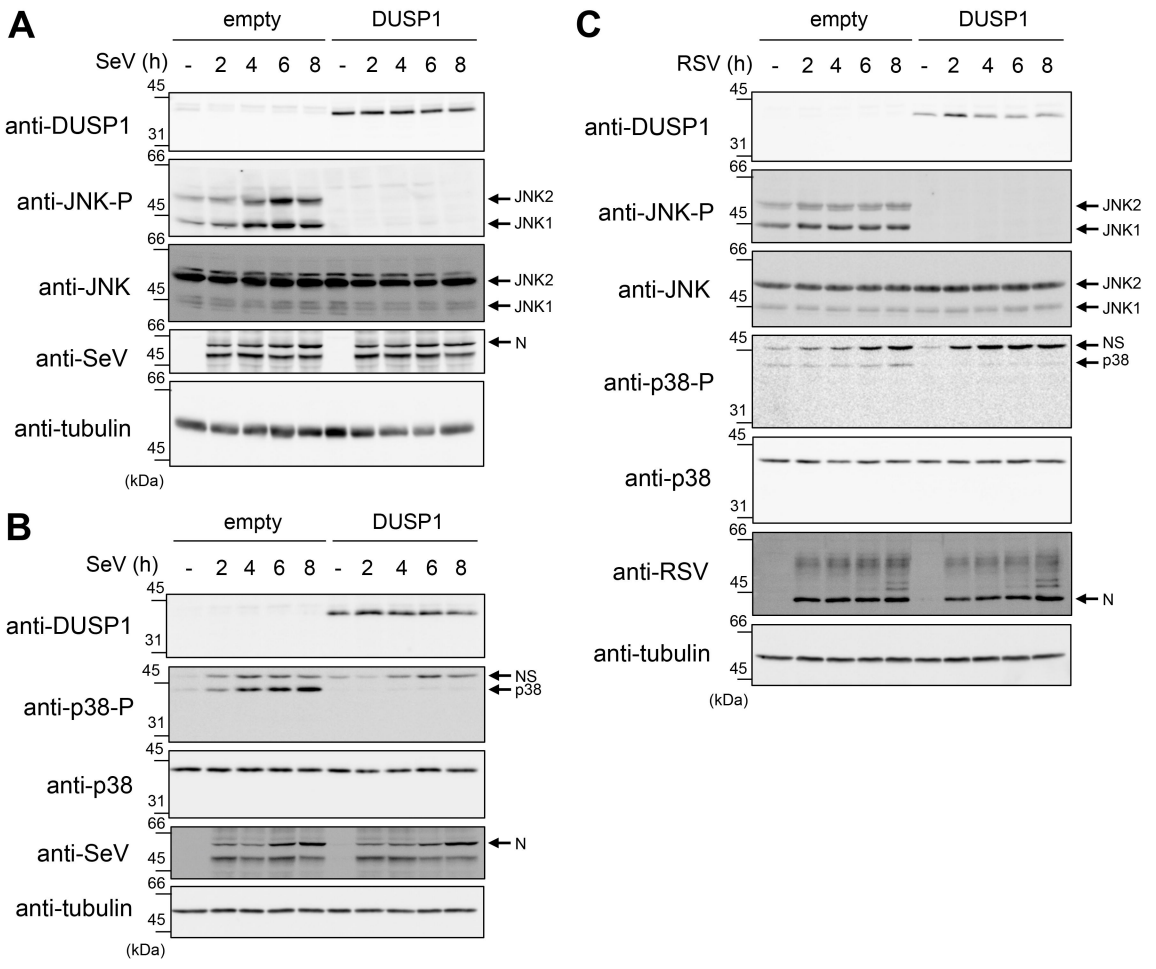
A
empty
DUSP1
SeV (h) - 2 4 6 8 - 2 4 6 8
anti-DUSP1
anti-JNK-P
anti-JNK
anti-SeV
anti-tubulin
JNK2
JNK1
N
(kDa)
B
empty
DUSP1
SeV (h) - 2 4 6 8 - 2 4 6 8
anti-DUSP1
anti-p38-P
anti-p38
anti-SeV
anti-tubulin
NS
p38
N
(kDa)
C
empty
DUSP1
RSV (h) - 2 4 6 8 - 2 4 6 8
anti-DUSP1
anti-JNK-P
anti-JNK
anti-p38-P
anti-p38
anti-RSV
anti-tubulin
JNK2
JNK1
NS
p38
N
(kDa)

Figure 4

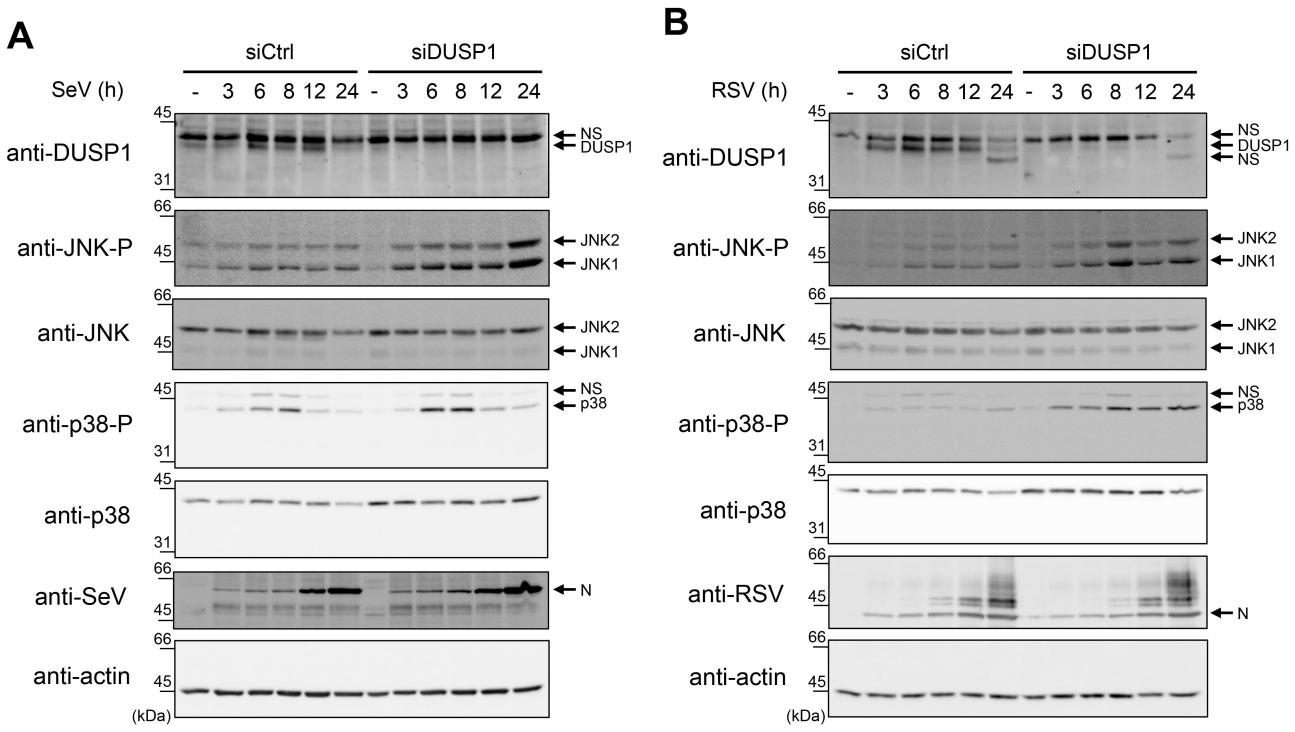
A
siCtrl
siDUSP1
SeV (h)
- 3 6 8 12 24 - 3 6 8 12 24
anti-DUSP1
NS
DUSP1
anti-JNK-P
JNK2
JNK1
anti-JNK
JNK2
JNK1
anti-p38-P
NS
p38
anti-p38
anti-SeV
N
anti-actin
(kDa)
B
siCtrl
siDUSP1
RSV (h)
- 3 6 8 12 24 - 3 6 8 12 24
anti-DUSP1
NS
DUSP1
NS
anti-JNK-P
JNK2
JNK1
anti-JNK
JNK2
JNK1
anti-p38-P
NS
p38
anti-p38
anti-RSV
N
anti-actin
(kDa)

Figure 5

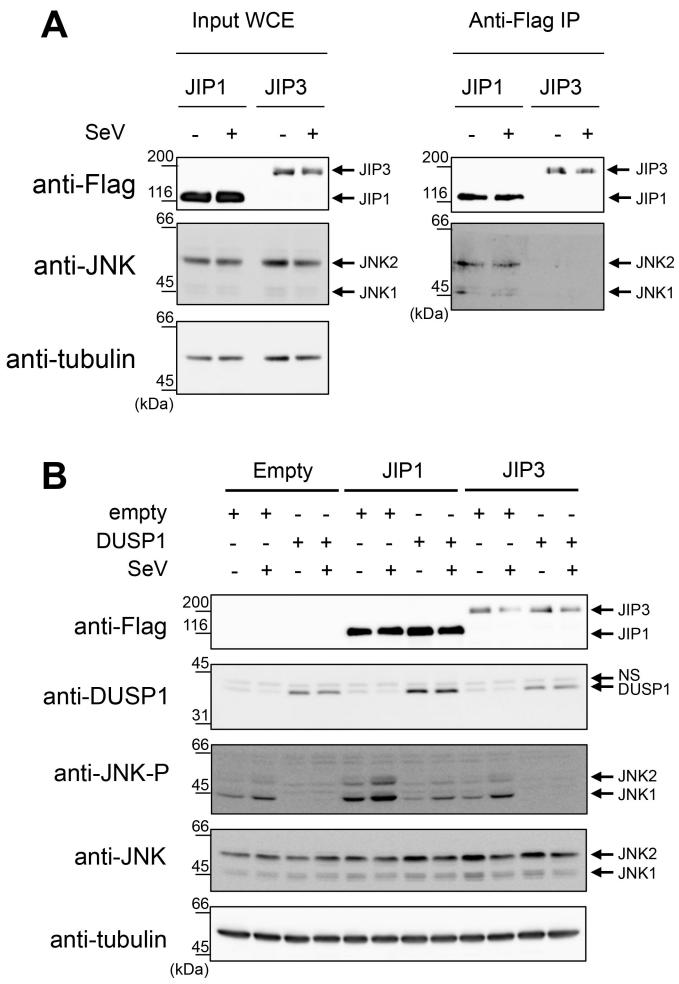
A
Input WCE
Anti-Flag IP
JIP1
JIP3
JIP1
JIP3
SeV
- + - +
- + - +
anti-Flag
anti-JNK
anti-tubulin
200
116
66
45
66
45
66
45
(kDa)
JIP3
JIP1
JNK2
JNK1
JIP3
JIP1
JNK2
JNK1
(kDa)
B
Empty
JIP1
JIP3
empty
DUSP1
SeV
+ + - - + + - - + + - -
- - + + - - + + - - + +
- + - + - + - + - + - +
anti-Flag
anti-DUSP1
anti-JNK-P
anti-JNK
anti-tubulin
200
116
45
31
66
45
66
45
66
45
(kDa)
JIP3
JIP1
NS
DUSP1
JNK2
JNK1
JNK2
JNK1

Figure 6

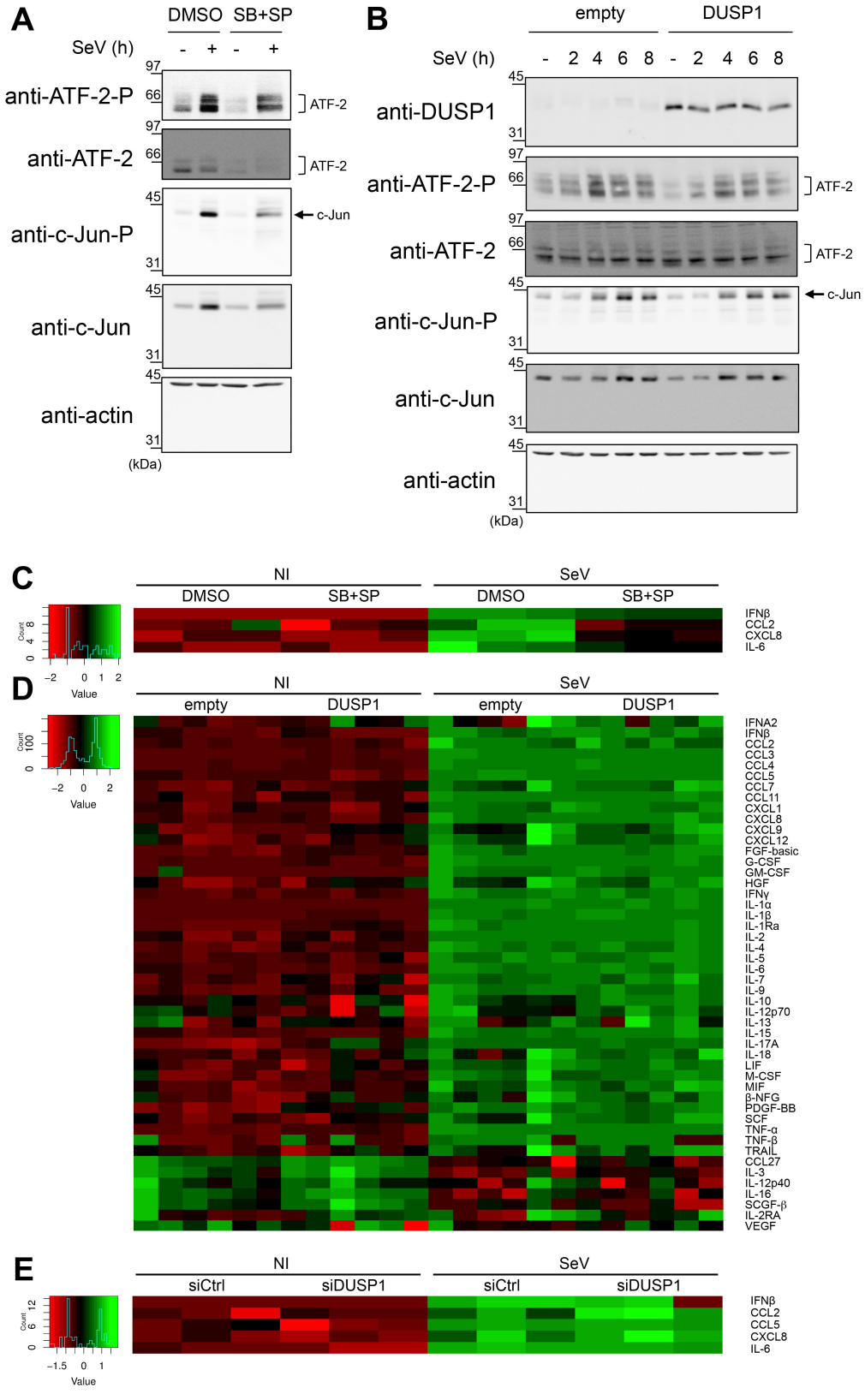
A
DMSO
SB+SP
SeV (h)
- + - +
anti-ATF-2-P
anti-ATF-2
anti-c-Jun-P
anti-c-Jun
anti-actin
ATF-2
c-Jun
(kDa)
B
empty
DUSP1
SeV (h)
- 2 4 6 8 - 2 4 6 8
anti-DUSP1
anti-ATF-2-P
anti-ATF-2
anti-c-Jun-P
anti-c-Jun
anti-actin
ATF-2
c-Jun
(kDa)
C
NI
SeV
DMSO
SB+SP
DMSO
SB+SP
IFNβ
CCL2
CXCL8
IL-6
Count
Value
D
NI
SeV
empty
DUSP1
empty
DUSP1
IFNA2
IFNβ
CCL2
CCL3
CCL4
CCL5
CCL7
CCL11
CXCL1
CXCL8
CXCL9
CXCL12
FGF-basic
G-CSF
GM-CSF
HGF
IFNγ
IL-1α
IL-1β
IL-1Ra
IL-2
IL-4
IL-5
IL-6
IL-7
IL-9
IL-10
IL-12p70
IL-13
IL-15
IL-17A
IL-18
LIF
M-CSF
MIF
β-NFG
PDGF-BB
SCF
TNF-α
TNF-β
TRAIL
CCL27
IL-3
IL-12p40
IL-16
SCGF-β
IL-2RA
VEGF
Count
Value
E
NI
SeV
siCtrl
siDUSP1
siCtrl
siDUSP1
IFNβ
CCL2
CCL5
CXCL8
IL-6
Count
Value

Figure 7

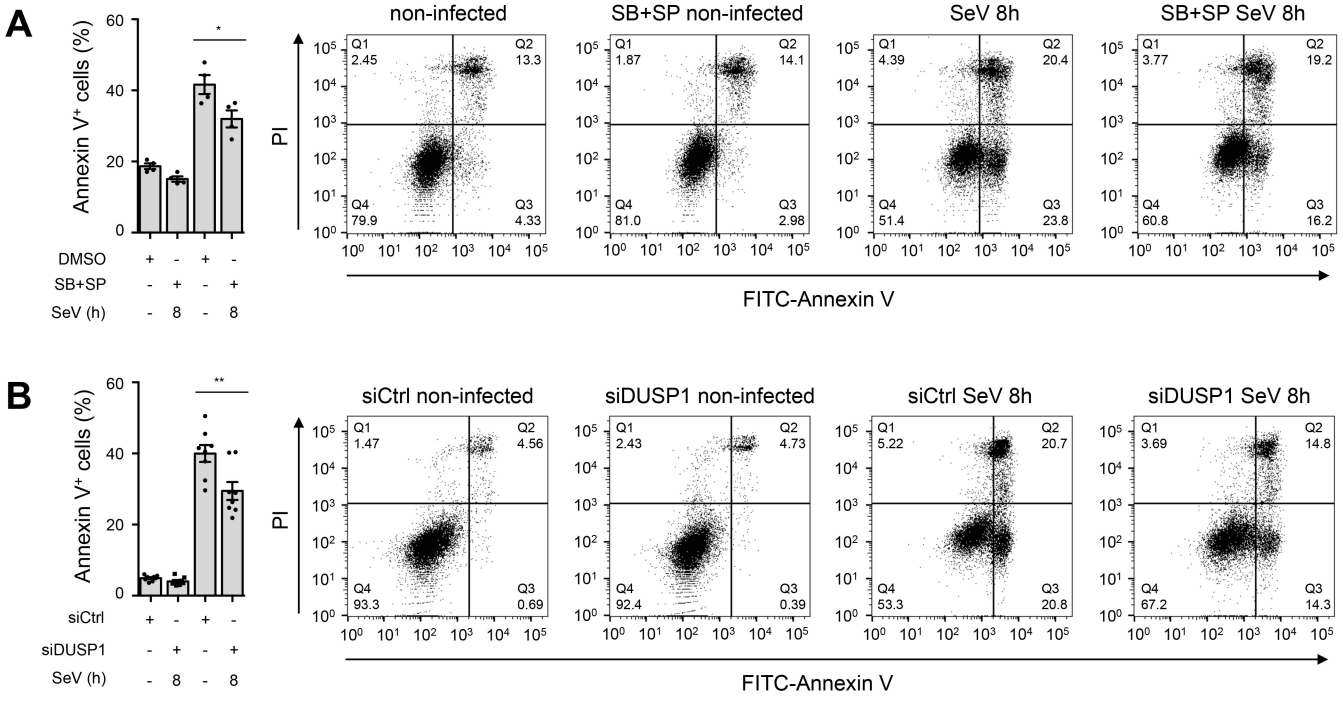
A
Annexin V+ cells (%)
60
40
20
0
*
DMSO + - + -
SB+SP - + - +
SeV (h) - 8 - 8
non-infected
SB+SP non-infected
SeV 8h
SB+SP SeV 8h
PI
Q1 2.45
Q2 13.3
Q4 79.9
Q3 4.33
Q1 1.87
Q2 14.1
Q4 81.0
Q3 2.98
Q1 4.39
Q2 20.4
Q4 51.4
Q3 23.8
Q1 3.77
Q2 19.2
Q4 60.8
Q3 16.2
FITC-Annexin V
B
Annexin V+ cells (%)
60
40
20
0
**
siCtrl + - + -
siDUSP1 - + - +
SeV (h) - 8 - 8
siCtrl non-infected
siDUSP1 non-infected
siCtrl SeV 8h
siDUSP1 SeV 8h
PI
Q1 1.47
Q2 4.56
Q4 93.3
Q3 0.69
Q1 2.43
Q2 4.73
Q4 92.4
Q3 0.39
Q1 5.22
Q2 20.7
Q4 53.3
Q3 20.8
Q1 3.69
Q2 14.8
Q4 67.2
Q3 14.3
FITC-Annexin V

Figure 8

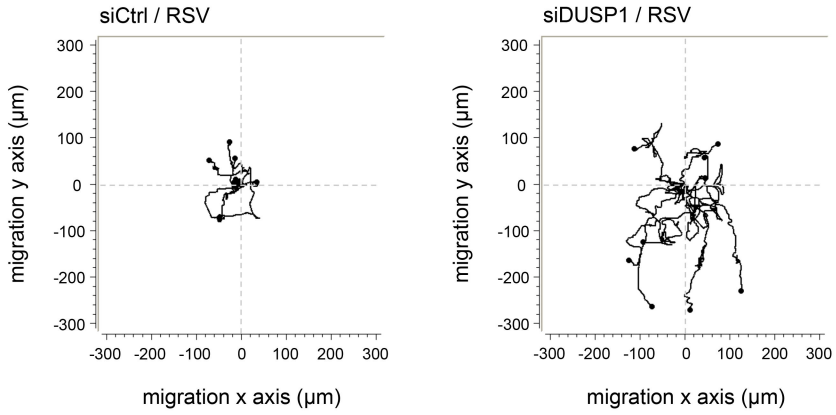
siCtrl / RSV
siDUSP1 / RSV
migration y axis (µm)
migration x axis (µm)
300
200
100
0
-100
-200
-300